Nonreciprocal Surface Acoustic Waves in Multilayers with Magnetoelastic and Interfacial Dzyaloshinskii-Moriya Interactions

Roman Verba,[1] Ivan Lisenkov,[2,3,*] Ilya Krivorotov,[4] Vasil Tiberkevich,[5] and Andrei Slavin[5]

[1]*Institute of Magnetism, Kyiv 03680, Ukraine*
[2]*School of Electrical Engineering and Computer Science, Oregon State University, Corvallis, Oregon 97333, USA*
[3]*Kotelnikov Institute of Radioengineering and Electronics, Russian Academy of Sciencies, Moscow 125009, Russia*
[4]*Department of Physics and Astronomy, University of California, Irvine, California 92697, USA*
[5]*Department of Physics, Oakland University, Rochester, Michigan 48309, USA*

(Received 29 December 2017; revised manuscript received 13 April 2018; published 12 June 2018)

Surface acoustic waves (SAWs) propagating in a piezoelectric substrate covered with a thin ferromagnetic–heavy-metal bilayer are found to exhibit a substantial degree of nonreciprocity, i.e., the frequencies of these waves are nondegenerate with respect to the inversion of the SAW propagation direction. The simultaneous action of the magnetoelastic interaction in the ferromagnetic layer and the interfacial Dzyaloshinskii-Moriya interaction in the ferromagnetic–heavy-metal interface results in the openings of magnetoelastic band gaps in the SAW spectrum, and the frequency position of these band gaps is different for opposite SAW propagation directions. The band-gap widths and the frequency separation between them can be controlled by a proper selection of the magnetization angle and the thickness of the ferromagnetic layer. Using numerical simulations, we demonstrate that the isolation between SAWs propagating in opposite directions in such a system can exceed the direct SAW propagation losses by more than 1 order of magnitude.

DOI: 10.1103/PhysRevApplied.9.064014

I. INTRODUCTION

Surface acoustic wave (SAW) transmission lines, based on high-quality piezoelectric single crystals, found applications as frequency filters, sensors, and other signal processing devices [1–4]. SAWs have very low propagation losses at frequencies ranging from a megahertz to several gigahertz. They can be excited with a very high efficiency in piezoelectric crystals, and the use of unidirectional transducers [3,4] can reduce the insertion losses of SAW transmission lines to just several decibels. Moreover, typical propagation speeds (and therefore wavelengths) of SAWs in crystals are several orders of magnitude less than the speed of electromagnetic waves, thus allowing a miniaturization of SAW signal processing devices compared to their electromagnetic counterparts.

A typical frequency spectrum $\omega_{\boldsymbol{k}}$ of a SAW is reciprocal, i.e., it is degenerate for SAWs having opposite wave vectors $\boldsymbol{k}$ and $-\boldsymbol{k}$: $\omega_{\boldsymbol{k}} = \omega_{-\boldsymbol{k}}$. This degeneracy is a result of a fundamental time-reversal symmetry in the laws of mechanics. However, frequency nonreciprocity (when $\omega_{\boldsymbol{k}} \neq \omega_{-\boldsymbol{k}}$) is extremely important for applications: it allows us to isolate signals traveling in opposite directions [5,6]. From a practical point of view, a good isolator should demonstrate high rejection; i.e., it should block most of the power traveling in one direction (say, from port 2 to port 1). Simultaneously, it should have low insertion loss, i.e. transmit nearly all of the power traveling in the opposite direction (from port 1 to port 2). It is known that SAW-based devices demonstrate very low transmission losses—and therefore should be useful as isolators—if a nonreciprocal propagation SAW propagation in these devices can be demonstrated.

Unfortunately, a nonreciprocal propagation of a SAW is not easy to achieve. Thus far, the nonreciprocal propagation of a SAW has been found in devices with moving or rotating elements [7,8], where the effect of the summation of velocities of sound and moving media was used. An alternative way to achieve acoustic nonreciprocity is to use nonlinear effects in high-power acoustic waves, where the acoustic wave loss or gain are power dependent [9–12]. Unfortunately, neither of these ways have led to the development of practical nonreciprocal devices based on acoustic waves.

In contrast to acoustic waves, the frequency nonreciprocity of spin waves (SWs) propagating in ferromagnetic media is not an exotic phenomenon. The SW nonreciprocity is a consequence of the intrinsic breaking of time-reversal

*ivan.lisenkov@phystech.edu

symmetry in magnetized magnetic materials, where magnetization precesses only clockwise around its equilibrium direction. The frequency nonreciprocity for SWs can be achieved in multiple ways, e.g., by nonsymmetric boundary conditions [13–15], by patterning of a ferromagnet [16–18], or by a bulk or interfacial Dzyaloshinskii-Moriya interaction [19–22]. It should be noted that the application of the SWs themselves for the development of compact nonreciprocal microwave devices is a challenging task, as the magnetic field bias is needed, and the problem of a relatively high SW propagation losses should be solved.

Fortunately, owing to the magnetoelastic interaction in magnetostrictive materials, the SWs and acoustic waves can interact with each other, and SWs can act as a "source" of nonreciprocity for acoustic waves. The nonreciprocity of magnetoelastic waves [23–25], as well as the magnetoelastic interaction itself [26–28], have been studied for a long time in the case of bulk samples. The bulk materials, however, typically do not show good acoustic, magnetic, magnetoelastic, and piezoelectric properties simultaneously, which hinders their practical applications in nonreciprocal devices. For example, many papers have been devoted to the study of magnetoelastic waves in yttrium iron garnet (YIG), which has nice magnetic properties, but the magnetoelastic interaction in YIG is weak, and this material has no piezoelectricity at all. At the same time, metallic ferromagnets (such as Ni, Co, and Fe) have rather large magnetostriction (3 to 4 orders larger than in YIG), but prohibitively bad acoustic properties.

Rather promising recent experiments [29–32] have demonstrated that the propagation of SAWs in piezoelectric substrates can be controlled by a thin magnetic layer placed atop the substrate. The use of such heterostructures allows one to combine in a single device a high-quality piezoelectric substrate (like $LiNbO_3$) and a ferromagnet with large magnetostriction (e.g., Ni). Moreover, it has been shown that SAWs propagating in a $LiNbO_3$ substrate covered by a thin Ni film indeed demonstrate some degree of nonreciprocity [32], although the observed nonreciprocity effect was small. In such a case, the SWs are generally reciprocal, and the small transmission nonreciprocity comes from the slightly different widths of the magnetoelastic band gaps having the same central frequency in the SAW spectrum for waves with opposite wave vectors. As a result, the nonreciprocal transmission appears on a background of large propagation (insertion) losses.

In this work, we propose a way to substantially enhance the nonreciprocal properties of SAW in piezoelectric-ferromagnetic heterostructures using the materials with the interfacial Dzyaloshinskii-Moriya interaction (IDMI). We show that the IDMI results in a nondegeneracy of the *central frequencies* of the magnetoelastic band gaps with respect to the inversion of the SAW propagation direction. Since the central frequencies of the band gaps are different for the two counterpropagating waves, a wave traveling in one direction falls within the band gap, while the wave traveling in the opposite direction does not "feel" the band gap at all. Therefore, the damping of the wave propagating in one direction is tremendously increased, while that for the wave propagating in the opposite direction is practically unaffected, resulting in the simultaneously high isolation and low insertion losses. In our numerical simulations, we use the parameters of a transmission line based on a $LiNbO_3$ substrate covered by a thin Ni/Pt bilayer, and we show that, using a high-quality Ni film, one can achieve an isolation of up to 45 dB with insertion losses of about 20 dB.

The article is organized as follows. In Sec. II, we present a general formalism for the magnetoelastic coupling between the linear SWs and SAWs in the framework of a perturbation theory. Then we consider the conditions for the appearance of nonreciprocal magnetoelastic band gaps in the wave spectrum (Sec. III B), and the ways for the optimization of the nonreciprocal properties (Sec. III C). Finally, Sec. III D is devoted to the calculation of the SAW line transmission characteristics in the presence of the IDMI and the SAW coupling to SWs.

II. THEORY OF WEAKLY COUPLED LINEAR MAGNETOELASTIC WAVES

In this section, we revisit the theory of magnetoelastic interactions in ferromagnetic samples, and we develop an analytical formalism for magnetoelastic coupling between the spin waves and acoustic waves suitable for the systems having arbitrary wave profiles (e.g., suitable for surface magnetoelastic waves), limiting ourselves to the case of linear coupling between SWs and SAWs.

The dynamics of the magnetoelastic waves is governed by the coupled Landau-Lifshitz equation for SWs and elastic mechanical equations [2,5] for acoustic waves. Simulations solution of these equations is complicated and is often possible only numerically [33–36]. However, in almost all of the practically important situations, the magnetostriction is weak in comparison to the other interactions in a ferromagnet, which allows us to consider the magnetoelastic interaction in the framework of perturbation theory.

For the consideration of linear excitations, the magnetization vector $\boldsymbol{M}$ can be represented as a sum of static and dynamic components, $\boldsymbol{M}(\boldsymbol{r},t) = M_s[\boldsymbol{\mu}(\boldsymbol{r}) + \boldsymbol{m}(\boldsymbol{r},t)]$, where M_s is the saturation magnetization, $\boldsymbol{\mu}$ is the unit vector pointing in the direction of the static magnetization, and $\boldsymbol{m}$ is a dimensionless dynamic magnetization ($|\boldsymbol{m}| \ll 1$). Then the equations describing the coupled magnetoelastic dynamics can be written as

$$\frac{1}{\gamma}\hat{\boldsymbol{J}}\cdot\frac{d\boldsymbol{m}(\boldsymbol{r},t)}{dt} - \int \hat{\boldsymbol{\Omega}}\cdot\boldsymbol{m}(\boldsymbol{r}',t)d\boldsymbol{r}' = \boldsymbol{b}^{\mathrm{me}}(\boldsymbol{r},t), \qquad (1)$$

$$\rho\frac{\partial^2}{\partial t^2}\xi_i(\boldsymbol{r},t)-c_{ijln}\frac{\partial^2}{\partial x_j\partial x_l}\xi_n(\boldsymbol{r},t)=f_i^{\mathrm{me}}(\boldsymbol{r},t). \quad (2)$$

Here, $\hat{\boldsymbol{J}}=\hat{\boldsymbol{e}}\cdot\boldsymbol{\mu}$ is the operator of the angular momentum, $\hat{\boldsymbol{e}}$ is the Levi-Cività antisymmetric tensor, $\hat{\boldsymbol{\Omega}}=\hat{\boldsymbol{\Omega}}(\boldsymbol{r},\boldsymbol{r}')$ is the operator of magnetic interactions (see Refs. [37–39] for additional details), $\boldsymbol{\xi}(\boldsymbol{r},t)$ is the elastic displacement, ρ is the density, and c_{ijlm} represents the components of the elastic stiffness tensor. The magnetoelastic coupling is given by the terms on the right-hand side of the equation, where $\boldsymbol{b}^{\mathrm{me}}(\boldsymbol{r},t)$ is the effective magnetic field generated by the acoustic deformations via the inverse magnetostriction, and $\boldsymbol{f}^{\mathrm{me}}$ is the effective force generated by the magnetization dynamics and acting on the sample via the direct magnetostriction effect. In Eq. (1), we skip another coupling term of the form $\boldsymbol{m}(\boldsymbol{\mu}\cdot\boldsymbol{b}^{\mathrm{me}})$, as it is of the second order of smallness and cannot result in a linear coupling between the waves. In Eq. (2) and below, the repeating indices $(i,j,l,m)=(x,y,z)$ are assumed to be summed.

The magnetoelastic coupling can be obtained from the following magnetoelastic energy density

$$W^{\mathrm{me}}=\frac{1}{M_s^2}b_{ijln}u_{ij}M_lM_n, \quad (3)$$

where $\hat{\boldsymbol{b}}$ is the tensor of magnetostriction [40] and $\hat{\boldsymbol{u}}(\boldsymbol{r},t)$ is the tensor defining the strain created by the displacement $\boldsymbol{\xi}(\boldsymbol{r},t)$ [2]

$$u_{ij}=\frac{1}{2}\left(\frac{\partial\xi_i}{\partial r_j}+\frac{\partial\xi_j}{\partial r_i}\right). \quad (4)$$

The values of the field $\boldsymbol{b}^{\mathrm{me}}$ and the force $\boldsymbol{f}^{\mathrm{me}}$ can be calculated using Eq. (3) as

$$b_n^{\mathrm{me}}(\boldsymbol{r},t)=-\frac{\partial W^{\mathrm{me}}}{\partial\boldsymbol{M}}\approx-\frac{2}{M_s}b_{ijln}u_{ij}(\boldsymbol{r},t)\mu_l(\boldsymbol{r}), \quad (5)$$

$$f_i^{\mathrm{me}}(\boldsymbol{r},t)=\frac{\partial}{\partial x_i}\frac{\partial}{\partial u_{ij}}W^{\mathrm{me}}\approx 2\frac{\partial}{\partial x_j}b_{ijln}\mu_l(\boldsymbol{r})m_n(\boldsymbol{r},t), \quad (6)$$

where we leave only the terms that are linear in the dynamic magnetization $\boldsymbol{m}$ or displacement $\boldsymbol{\xi}$, as they are responsible for the linear coupling between the waves. The other terms, corresponding, e.g., to the parametric coupling between the waves, are disregarded.

Equations (1) and (2) can be solved within a standard framework of an eigenmode expansion:

$$\boldsymbol{m}(\boldsymbol{r},t)=\sum_\nu c_\nu(t)\boldsymbol{m}_\nu(\boldsymbol{r})+\mathrm{c.c.}, \quad (7)$$

$$\boldsymbol{\xi}(\boldsymbol{r},t)=\sum_\lambda q_\lambda(t)\boldsymbol{\xi}_\lambda(\boldsymbol{r})+\mathrm{c.c.}, \quad (8)$$

where $\boldsymbol{m}_\nu(\boldsymbol{r})$ and $\boldsymbol{\xi}_\lambda(\boldsymbol{r})$ are the profiles of the linear SWs and acoustic modes, while $c_\nu(t)$ and $q_\lambda(t)$ are the unknown complex amplitudes of the eigenmodes. The spatial profiles of the eigenmodes and their eigenfrequencies, ω_ν and $\tilde{\omega}_\lambda$, respectively, are the solutions of Eqs. (1) and (2) with zero right-hand-side parts in the form $\boldsymbol{m}(\boldsymbol{r},t)=\boldsymbol{m}_\nu(\boldsymbol{r})e^{-i\omega_\nu t}$, while $\boldsymbol{\xi}(\boldsymbol{r},t)=\boldsymbol{\xi}_\lambda(\boldsymbol{r})e^{-i\tilde{\omega}_\lambda t}$.

The linear SW modes satisfy the following orthogonality relation [37,38]

$$\frac{M_s}{\gamma}\int\boldsymbol{m}_{\nu'}^*(\boldsymbol{r})\cdot\boldsymbol{\mu}(\boldsymbol{r})\times\boldsymbol{m}_\nu(\boldsymbol{r})d\boldsymbol{r}=-iA_\nu\delta_{\nu,\nu'}, \quad (9)$$

where $A_\nu>0$ is the spin-wave normalization constant having the dimensionality of action [41]. A similar orthogonality condition can be written for the acoustic modes [2,42]

$$2\omega_\lambda\int\rho(\boldsymbol{r})\boldsymbol{\xi}_\lambda^*(\boldsymbol{r})\cdot\boldsymbol{\xi}_{\lambda'}(\boldsymbol{r})d\boldsymbol{r}=Q_\lambda\delta_{\lambda\lambda'}, \quad (10)$$

where $Q_\lambda>0$ is a positive normalization constant having the same dimensionality as A_ν.

Substituting the expansion equations (7) and (8) for $\boldsymbol{m}(\boldsymbol{r},t)$ and $\boldsymbol{\xi}(\boldsymbol{r},t)$ into Eqs. (1) and (2) and using the orthogonality relations, we get the following final equations for the amplitudes of the coupled spin and acoustic waves:

$$\begin{aligned}\frac{dc_\nu}{dt}+i\omega_\nu c_\nu+\Gamma_\nu c_\nu&=i\sum_\lambda\sqrt{\frac{Q_\lambda}{A_\nu}}\kappa_{\nu,\lambda}q_\lambda,\\ \frac{dq_\lambda}{dt}+i\tilde{\omega}_\lambda q_\lambda+\tilde{\Gamma}_\lambda q_\lambda&=i\sum_\nu\sqrt{\frac{A_\nu}{Q_\lambda}}\kappa_{\nu,\lambda}^*c_\nu,\end{aligned} \quad (11)$$

where we also introduce in a common way [8,38] the damping rates of the spin and acoustic modes Γ_ν and $\tilde{\Gamma}_\lambda$, respectively. The coupling coefficient is equal to

$$\kappa_{\nu,\lambda}=\frac{2}{\sqrt{A_\nu Q_\lambda}}\int\boldsymbol{\mu}(\boldsymbol{r})\cdot[\hat{\boldsymbol{b}}\cdot\hat{\boldsymbol{u}}_\lambda(\boldsymbol{r})]\cdot\boldsymbol{m}_\nu^*(\boldsymbol{r})d\boldsymbol{r}. \quad (12)$$

This expression is the central result of the above-developed theory. The coupling coefficient can be calculated for the arbitrary spatial profiles of the acoustic and SW modes. The exact profiles of the SW and acoustic modes, as well as the mode eigenfrequencies ω_ν and $\tilde{\omega}_\lambda$, in simple cases can be found analytically or, otherwise, can be extracted from numeric simulations.

In the case of propagating waves, characterized by a wave vector $\boldsymbol{k}$, the solution of Eq. (11) can be easily obtained. In the equations above, we change $\boldsymbol{m}_\nu\to\boldsymbol{m}_{\boldsymbol{k}}(\boldsymbol{\rho})e^{i\boldsymbol{k}\cdot\boldsymbol{r}}$ and $\boldsymbol{\xi}_\lambda\to\boldsymbol{\xi}_{\boldsymbol{k}'}(\boldsymbol{\rho})e^{i\boldsymbol{k}'\cdot\boldsymbol{r}}$, where $\boldsymbol{\rho}$ is two-dimensional radius vector, perpendicular to the wave propagation direction, defined by $\boldsymbol{k}$. Then Eq. (12) is transformed to

$$\kappa_{\boldsymbol{k},\boldsymbol{k}'} = \frac{2}{\sqrt{A_{\boldsymbol{k}} Q_{\boldsymbol{k}'}}} \int \boldsymbol{\mu}(\boldsymbol{r}) \cdot [\hat{\boldsymbol{b}} \cdot \hat{\boldsymbol{u}}_{\boldsymbol{k}'}(\boldsymbol{\rho})] \cdot \boldsymbol{m}^*_{\boldsymbol{k}}(\boldsymbol{\rho}) e^{i(\boldsymbol{k}'-\boldsymbol{k})\cdot\boldsymbol{r}} d\boldsymbol{r}. \tag{13}$$

It is clear that, in the case when the static magnetization is uniform along the wave propagation direction, the exponent under the integral gives a zero integration result until $\boldsymbol{k} \neq \boldsymbol{k}'$. Therefore, in this case, the spin and acoustic waves can interact only if they have the same wave vector $\boldsymbol{k}$. Note that the length L of the sample in the wave propagation direction, which appears after the integration in Eq. (13), is canceled out by the same term in the normalization constants of the SW and the SAW. The dispersion relation for the interacting waves can be written as

$$\omega_k = \frac{\omega_{\mathrm{SW}} + \omega_{\mathrm{AW}}}{2} \pm \sqrt{\left(\frac{\omega_{\mathrm{SW}} - \omega_{\mathrm{AW}}}{2}\right)^2 + |\kappa_k|^2}, \tag{14}$$

where $\omega_{\mathrm{SW}} = \omega_{\mathrm{SW},\boldsymbol{k}}$ and $\omega_{\mathrm{AW}} = \omega_{\mathrm{AW},\boldsymbol{k}}$ are the dispersion relations of the noninteracting SWs and acoustic waves, respectively.

III. NONRECIPROCAL SURFACE MAGNETOELASTIC WAVES

A. Spin-wave modes in a ferromagnetic film with the IDMI

In this section, we apply the above-presented general theory to the study of the surface magnetoelastic waves in a magnetic-nonmagnetic heterostructure. A sketch of a considered heterostructure is shown in Fig. 1. It consists of a nonmagnetic substrate which supports the propagation of a SAW. Typically, this substrate is a piezoelectric single crystal, like $LiNbO_3$, $LiTaO_3$ or quartz. The piezoelectric substrate is covered with a thin ferromagnetic film having a large magnetostriction (e.g., Ni), and then by a thin heavy-metal layer (typically Pt), which induces the IDMI at the ferromagnetic–heavy-metal interface. The ferromagnetic layer is biased by an external magnetic field $\boldsymbol{B}_e$ applied in the film plane at the angle ϕ with respect to the wave propagation direction. The value of the bias field should be sufficient to saturate the ferromagnetic film in its plane, thus overcoming the effect of the surface perpendicular magnetic anisotropy, which can exist at the ferromagnetic–heavy-metal interface.

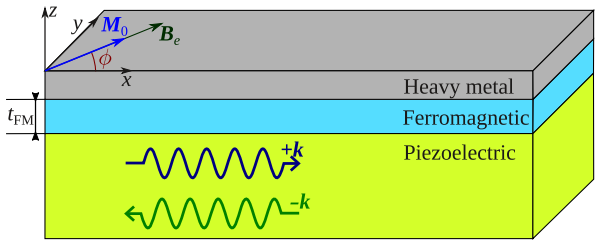

FIG. 1. A layout of the heterostructure under study, a piezoelectric substrate covered by a ferromagnetic–heavy-metal bilayer.

Since the IDMI is an interface effect, the thickness of a ferromagnetic film necessary to produce a significant SW nonreciprocity should be sufficiently small. As has become clear from the results of our numerical simulations, the ferromagnetic film thickness should not exceed several tens of nanometers. In this case, we can use the assumption of a uniform SW profile across the thickness of a ferromagnetic layer, $\boldsymbol{m}_{\boldsymbol{k}} \notin f(z)$. The dispersion of SWs propagating along the x axis (see Fig. 1) can be expressed as [20,43]

$$\omega_{\mathrm{SW},k} = \sqrt{\Omega_{zz}\Omega_{\mathrm{IP}}} - \omega_M \tilde{D} k \sin\phi, \tag{15}$$

where

$$\begin{aligned} \Omega_{\mathrm{IP}} &= \omega_H + \omega_M[\lambda^2_{\mathrm{ex}} k^2 + f(kt)\sin^2\phi], \\ \Omega_{zz} &= \omega_H - \omega_{\mathrm{an}} + \omega_M[\lambda^2_{\mathrm{ex}} k^2 + 1 - f(kt)]. \end{aligned} \tag{16}$$

In these equations, $\omega_H = \gamma B_e$, $\omega_M = \gamma\mu_0 M_s$, and $\omega_{\mathrm{an}} = 2\gamma K_s/(M_s t_{\mathrm{FM}})$, where K_s is the constant of the surface perpendicular anisotropy, $k = k_x$, $f(x) = 1 - (1 - e^{-|x|})/|x|$ is a function describing the dynamic demagnetization, and the effect of the IDMI is described by the expression $\tilde{D} = 2Db/(\mu_0 M_s^2 t_{\mathrm{FM}})$, where D is the IDMI constant, t_{FM} is a thickness of the ferromagnetic layer, and b is the thickness of an atomic monolayer of the ferromagnet [21,44]. From Eq. (15), it is clear that the SW dispersion is nonreciprocal: $\omega_{\mathrm{SW},k} \neq \omega_{\mathrm{SW},-k}$ if $\phi \neq 0, \pi$. Because of the symmetry of the effective field, produced by the IDMI, the vector structure of the SW mode does not depend on the IDMI [43], and it can be expressed as $\boldsymbol{m}_k = [-m_{\mathrm{IP}} \sin\phi, m_{\mathrm{IP}} \cos\phi, im_z]$, where m_{IP} is the in-plane dynamic component of magnetization, and the relation between the magnetization dynamic components is $m_z/m_{\mathrm{IP}} = \sqrt{\Omega_{\mathrm{IP}}/\Omega_{zz}}$.

B. Analysis of the coupling of surface acoustic waves with spin waves

The calculation of a dispersion relation and mode profile of SAWs in a layered structure consisting of a piezoelectric substrate and a metallic layer is, in itself, not a simple task. Thus, to simplify our analytical analysis, we use several approximations. First, we consider the substrate as isotropic and nonpiezoelectric and use the Poisson ratio as an adjustable parameter, as is often done in analytical calculations [1]. Within this approximation, it is not possible to answer the question on the SAW stability, but it is possible to adequately describe the profile of the SAW mode and, therefore, to evaluate the main characteristics of the magnetoelastic coupling of the SAWs and SWs.

Second, we neglect the influence of the thin metallic layer on the SAW properties. In general, shear acoustic waves in sputtered metals are slower than the shear acoustic waves in piezoelectric single crystals. Thus, in such a

system, the substrate is loaded by the metal layer, and the surface acoustic wave does not have any cutoff wave numbers [2,45,46]. In reality, the thickness of the ferromagnetic layer is on the order of $t_{\mathrm{Ni}} \approx 10$ nm, and the layer of the heavy metal can be as thin as 2 to 3 nm because the further increase of the heavy-metal thickness does not affect the strength of the IDMI [47]. The SAW wave number for the considered range of frequencies (1–5 GHz) is on the order of $k_x < 10\ \mu\mathrm{m}^{-1}$. Thus, we can work in an approximation in which $k_x(t_{\mathrm{Ni}} + t_{\mathrm{Pt}}) \ll 1$, and we assume that the SAW is only weakly affected mechanically by the bilayer. Therefore, we can use the wave dispersion and the wave mode profiles calculated for a free substrate [2,45]. It should be noted that the above-presented formalism (Sec. II) remains valid if one considers the exact values of both the acoustic field distribution and the SAW dispersion. This property could be useful in the future for making more-accurate calculations of the coupling parameter κ.

Taking into account the above-described approximations, we consider a Rayleigh surface acoustic wave [48]. The in-plane component of the displacement perpendicular to the SAW propagation direction is absent, $\xi_y = 0$, so the strain tensor components $u_{xy} = u_{yz} = u_{yy} = 0$. The oscillations in the x and z directions are shifted in phase by $\pi/2$, resulting in an effective rotation in the medium over an elliptic trajectory.

The only nonzero components of the SAW strain tensor are u_{xx}, u_{zz}, and u_{xz}. At the surface ($z = 0$ in Fig. 1), the off-diagonal strain component vanishes, $u_{xz}(z = 0) = 0$, while the components u_{xx} and u_{zz} remain nonzero. The dispersion of the SAW is linear, $\omega_{\mathrm{SAW},k} = c_{\mathrm{SAW}}|k|$, where c_{SAW} is the SAW velocity.

The magnetoelastic coupling tensor $\hat{\boldsymbol{b}}$ in the case of a cubic crystal (Ni, Fe, or Co) has only two independent components [5]: $b_{iiii} = b_1$ and $b_{ijij} = b_2$ (for $i \neq j$), while all of the other components are zero (in the case of an isotropic media $b_1 = b_2$). Noting the symmetry of the magnetoelastic tensor, we calculate the coupling coefficient κ_k for a SW in the ferromagnet and a Rayleigh SAW using Eq. (12):

$$\kappa_k = \frac{2t_{\mathrm{FM}}}{\sqrt{A_k Q_k}}\left[-b_1 \bar{u}_{xx,k} m^*_{\mathrm{IP},k} \sin\phi + b_2 \bar{u}_{xz,k} m^*_{z,k}\right]\cos\phi, \tag{17}$$

where $\bar{u}_{ij}$ represents the strain components, averaged over the ferromagnetic film thickness, and, in the definition of the normalization constants A_k and Q_k [Eqs. (9) and (10)], the integration over the volume is replaced by the integration over the z coordinate.

It is clear from Eq. (17) that the magnetoelastic interaction between the SW and SAW vanishes for $\phi = \pi/2$, while this angle corresponds to the maximum IDMI-induced SW nonreciprocity; see Eq. (15). As was pointed out earlier, at the free surface, the strain component $u_{xz} = 0$, so the averaged value $|\bar{u}_{xz}| \ll |\bar{u}_{xx}|$, and the coupling coefficient is determined mainly by the first term in brackets in Eq. (17). Therefore, the coupling coefficient is approximately proportional to the function $\kappa_k \sim \sin 2\phi$, which reaches its maximum at $\phi = \pi/4$. Consequently, the maximal coupling of SW and SAW is realized for the magnetization angle close to $\phi = \pi/4$. This feature has been already observed in Refs. [29,32].

We also note that the SW eigenmode does not change with the reversal of the propagation direction $\boldsymbol{m} = \boldsymbol{m}_{-k}$. At the same time, the SAW strain tensor transforms as $u_{xx,-k} = -u_{xx,k}$, $u_{xz,-k} = u_{xz,k}$ [48]. Therefore, the coupling between the SW and the SAW is nonreciprocal even without the IDMI, $\kappa_k \neq \kappa_{-k}$ (if $\phi \neq 0, \pi/2$), and this nonreciprocity becomes more pronounced for thicker ferromagnetic film due to an increase in the $\bar{u}_{xz}$ component. Unequal coupling results in different propagation losses of SAW in opposite directions, which was observed in Ref. [32]. However, to achieve a good isolation, while maintaining a low insertion loss, one should have $|\kappa_k| \ll |\kappa_{-k}|$. A simple analysis from Eq. (17) reveals that this requirement leads to the requirement on the stain distribution that $\bar{u}_{xx} \approx \bar{u}_{xz}$, which can be realized if ferromagnetic film thickness becomes of the order of the SAW penetration depth. For metallic layers, this requirement is difficult to fulfill because a thick ferromagnetic layer significantly affects the mechanical properties of the substrate and increases the acoustic loss. However, this regime may possibly be implemented in dielectric single-crystal ferromagnets, such as YIG.

C. Wave spectrum and magnetoelastic band gaps

For our numerical example demonstrating nonreciprocal surface magnetoelastic waves, we choose a $LiNbO_3$/Ni/Pt heterostructure. $LiNbO_3$/Ni heterostructures have already been fabricated and studied in Refs. [29,32], and they have demonstrated good magnetoelastic coupling. $LiNbO_3$ is one of the best piezoelectric materials supporting SAW propagation in a frequency range of up to 10 GHz [49], while Ni shows large magnetostriction, and the combination Ni/Pt gives the largest IDMI among the studied combinations of Ni with other heavy metals. We use the Y cut of $LiNbO_3$ having the density $\rho = 4650\ \mathrm{kg/m^3}$ as a substrate, and the SAW propagates along the Z axis. The substrate had the following material parameters: longitudinal and transversal sound velocities $c_l = 7350$ m/s and $c_t = 3600$ m/s [50], and the corresponding SAW velocity is $c_{\mathrm{SAW}} = 3361$ m/s. For the Ni layer, we use the following parameters: saturation magnetization $\mu_0 M_s = 0.66$ T, exchange stiffness $A = 9.5 \times 10^{-12}\ \mathrm{J/m^3}$ ($\lambda_{\mathrm{ex}} = 7.4$ nm), surface perpendicular anisotropy energy $K_s = 6 \times 10^{-4}\ \mathrm{J/m^2}$, g factor $g = 2.21$, magnetoelastic coupling coefficients $b_1 = 9.38\ \mathrm{MJ/m^3}$, $b_2 = 10\ \mathrm{MJ/m^3}$ [51,52]. The IDMI energy at the Pt-Ni interface is equal to

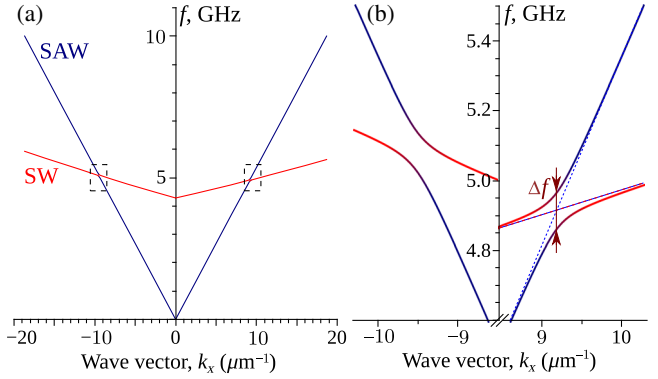

FIG. 2. (a) Spectra of surface magnetoelastic waves in the $LiNbO_3$/Ni/Pt heterostructure that, away from the points of wave hybridization, look like independent crossing spectra of the SAW and the SW, respectively. (b) Close-up of the spectra near the hybridization points [marked by dashed rectangles in (a)], where the magnetoelastic band gaps are clearly seen. Ni thickness, $t_{Ni} = 10$ nm; magnetization angle, $\phi = \pi/4$; bias field, $B_e = 41$ mT.

$D = -2.7 \times 10^{-3}$ J/m^2, while the lattice constant is $b = 0.352$ nm [53].

An example of the spectra of SW and SAW in the heterostructure is shown in Fig. 2. By selection of the magnitude of B_e and the angle ϕ of the bias magnetic field, it is possible to achieve a crossing between the spectra of the noninteracting SW and SAW in a desirable frequency range. The interaction between the SAW and the SW leads to the opening of band gaps in the spectrum of a magnetoelastic surface wave. The widths of the band gaps are determined by the coupling coefficient κ_k: $\Delta\omega = 2\pi\Delta f = 2|\kappa_k|$. Since the SW spectrum is nonreciprocal, the crossing of the SW dispersion curves with the SAW spectrum takes place at different points, and the magnetoelastic band gaps open at *different frequencies and wave numbers* for waves propagating in opposite directions. This feature is clearly visible in Fig. 2(b), where the central frequencies of the band gaps are shifted by 170 MHz with respect to each other. Therefore, within the frequency range of one of the band gaps, the SAW propagating in one direction is strongly coupled to the SW, forming a slow and dissipative magnetoelastic wave, while the wave traveling in the opposite direction is almost unaffected by the magnetoelastic interaction. This property exists due only to the SW frequency nonreciprocity induced by the IDMI in our case.

The widths of the band gaps and the separation between their central frequencies depend on the thickness of the ferromagnetic layer. The width Δf of a band gap increases with the thickness of the Ni layer t_{Ni} because the coupling coefficient between the SW and the SAW is proportional to t_{Ni}; see Eq. (17). However, because of the interfacial nature of the IDMI, the nonreciprocity of the SWs—and, therefore, the frequency separation between the band gaps

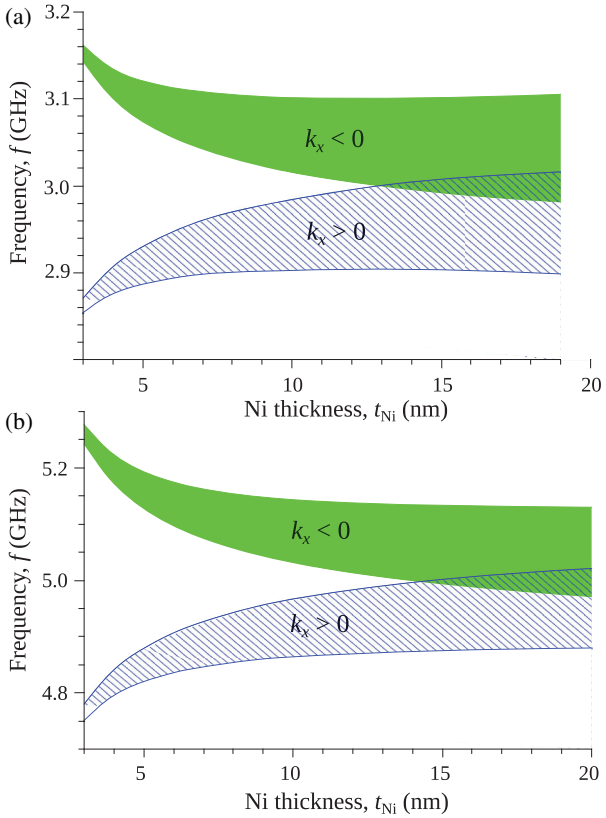

FIG. 3. Positions and widths of the magnetoelastic band gaps in a spectrum of surface magnetoelastic waves for opposite propagation directions. (a) Average frequency of 3 GHz. (b) Average frequency of 5 GHz. The magnetization angle is optimum, $\phi = \pi/4$.

corresponding to the opposite propagation directions—decreases with an increase in Ni thickness. These tendencies are clearly illustrated in Fig. 3, where the positions and the widths of the band gaps are plotted as functions of t_{Ni}. The bias field at each value of t_{Ni} is chosen in such a way that the average frequency position of the band gaps is kept constant [3 GHz in Fig. 3(a) and 5 GHz in Fig. 3(b), respectively]. For applications, it is desirable to have the widest possible band gaps, which, however, should be well separated from one another, at least by a frequency interval on the order of the band-gap width. Thus, there is an optimum range of ferromagnetic film thickness in which it is possible to achieve the best nonreciprocal properties of the magnetoelastic surface waves propagating in opposite directions. For example, in the above-described heterostructure $LiNbO_3$/Ni/Pt, the optimum thickness of the Ni layer is $t_{Ni} \approx 8$ to 9 nm for average frequencies of both 3 and 5 GHz (see Fig. 2). For higher average frequencies, the optimum Ni thickness remains almost the same, at least up to a frequency of 10 GHz, at which the SAW excitation and propagation in $LiNbO_3$ were observed experimentally in Ref. [49].

It should be noted that the crossing and hybridization of the dispersion curves of the SW and the SAW at any

desirable frequency cannot always be satisfied for the optimum magnetization angle of $\phi = \pi/4$. For example, for $t_{\mathrm{Ni}} > 19$ nm, the crossing cannot be achieved at a frequency below 3 GHz for any value of the bias field. This property is related to the increase of SW group velocity at $k \to 0$ taking place with the increase of film thickness. A solution of this problem is to use a smaller magnetization angle, $\phi < \pi/4$, which decreases the SW group velocity, and even changes its sign for $\sin^2\phi < \omega_H/(\omega_H + \omega_M - \omega_{\mathrm{an}})$. At such a magnetization angle, one can achieve the formation of magnetoelastic band gaps at almost any desirable frequency. However, the widths of the band gaps, as well as the separations between them, become smaller [see Eqs. (15) and (17)]. This feature limits the applicability of the IDMI-induced nonreciprocity of surface magnetoelastic waves in a relatively low-frequency range (below 2 GHz).

D. Transmission characteristics

In this section, we consider how the appearance of the magnetoelastic band gaps affects the transmission characteristics of a SAW line. In general, the appearance of the band gaps leads to a variation in the wave group velocity $v_{\mathrm{gr}} = \partial\omega_k/\partial k$ (the slope of the dispersion curve), and to a variation in the wave damping rate in the vicinity of the band gaps. Both of these factors contribute to the variation of a transmission rate in a magnetoacoustic transmission line.

It should be noted that common methods of SAW transmission calculations (see, e.g., Refs. [1,54]) are not applicable in our case. These methods use the assumption of a negligibly small resonance linewidth so that the wave group velocity and the efficiency of interdigital transducers (IDTs) can be calculated locally, at the point $k = k(\omega)$. This assumption is natural for SAWs, which typically have a very small linewidth (for example, for $LiNbO_3$, this linewidth is only 500 kHz at the 5-GHz frequency [55]). However, the SW damping rate—and, consequently, the damping rate of magnetoelastic waves in the vicinity of the band gaps—can be comparable to (or larger than) the band-gap width. In such a case, the nonresonant wave excitation becomes important, and one should integrate contributions from all of the excited waves within the resonance line.

To calculate the transmission characteristics, we need to introduce into Eq. (11) an external harmonic force which describes the excitation of SAWs by an IDT. The application to an IDT of a microwave voltage $V(t) = V_{\mathrm{in}}e^{-i\omega t}$ of the frequency ω results in the appearance of a mechanical force in the $LiNbO_3$ substrate, and this force has a certain spatial profile which depends on the IDT geometry. The efficiency of the coupling of IDT to a SAW having a certain wave vector $\boldsymbol{k} = k\boldsymbol{e}_x$ can be decomposed into two terms.

The first of these terms is the normalized Fourier transform F_k of the force spatial profile in the x direction, which determines the k dependence of the excitation efficiency. This term is often approximated by a function $F_k = \mathrm{sinc}[\pi N_f(k - k_0)/k]$, where N_f is the number of fingers in the IDT and $\omega_0 = c_{\mathrm{SAW}}k_0$ is the central frequency of the IDT [54].

The second term describes all of the other effects: piezoelectric coupling, overlap of the mechanical force with SAWs (in the z direction), etc. A detailed consideration of this second term lies beyond the scope of this article, and the influence of this second term is described below by a coefficient C_1. The coefficient C_1 can also be k dependent, but this dependence is much weaker than that of the term F_k and therefore is neglected below. Thus, the excitation force, which appears on the right-hand side of the equation for the SAW amplitudes q_k in the system equation (11), is expressed as $f_e(t) = C_1V_{\mathrm{in}}F_ke^{-i\omega t}$. The solution of Eq. (11) with the excitation term gives the amplitudes of the excited SAWs q_k in the form

$$q_k = -iC_1V_{\mathrm{in}}F_k\frac{\omega - (\omega_{\mathrm{SW}} - i\Gamma_{\mathrm{SW}})}{(\omega - \omega_1)(\omega - \omega_2)}, \tag{18}$$

where

$$\omega_{1,2} = \frac{\omega_{\mathrm{SW}} - i\Gamma_{\mathrm{SW}} + \omega_{\mathrm{SAW}} - i\Gamma_{\mathrm{SAW}}}{2} \pm \sqrt{\left[\frac{(\omega_{\mathrm{SW}} - i\Gamma_{\mathrm{SW}}) - (\omega_{\mathrm{SAW}} - i\Gamma_{\mathrm{SAW}})}{2}\right]^2 + |\kappa_k|^2}, \tag{19}$$

and the obtained frequencies of the coupled waves are complex because damping is taken into account.

At the receiving IDT, the displacement created by a SAW $\boldsymbol{\xi}(x) = (1/2\pi)\int \boldsymbol{\xi}_k q_k e^{ikx}dk$ is transformed into the output voltage via the piezoelectric effect. Similar to the excitation efficiency, the efficiency of detection of a SAW having the wave vector $\boldsymbol{k}$ can be decomposed into two terms and then, similar to the description of the efficiency at the input IDT, represented as C_2F_k. The total output microwave voltage is obtained by the integration over all of the SAW wave vectors, $V_{\mathrm{out}} = (C_2/2\pi)\int F_kq_ke^{ikL}dk$, where L is the distance between the input and output IDTs. Thus, the transmission parameters S_{12} and S_{21}, which are defined as ratios of the output voltage to the input one for the two opposite directions of the signal propagation (from port 1 to port 2, and vice versa) are equal to

$$S_{12,21} = \frac{C_1C_2}{2\pi i}\int \frac{\omega - (\omega_{\mathrm{SW}} - i\Gamma_{\mathrm{SW}})}{(\omega - \omega_1)(\omega - \omega_2)}F_k^2e^{\pm ikL}dk, \tag{20}$$

where S_{12} differs from S_{21} by the sign in front of the length L of the SAW line, and both IDTs are assumed to be the same. In a general case, this expression cannot be further simplified because the widths of the magnetoelastic band gaps, the SW damping rate, and the characteristic width of the function F_k can be on the same order of magnitude. In

the limiting case of the absence of magnetoelastic coupling and a sufficiently wide spectrum of the IDT (i.e., in the case where the range of variation of the function F_k is much larger than $\Gamma_{\mathrm{SAW}}/c_{\mathrm{SAW}}$), Eq. (20) simplifies to the form $S_{12,21} = (C_1C_2/c_{\mathrm{SAW}})\exp[-\Gamma_{\mathrm{SAW}}L/c_{\mathrm{SAW}}]$. The calculation of the coefficients C_1 and C_2 requires an accurate accounting of the piezoelectric coupling and impedance matching between the SAW line and the external circuit and lies beyond the scope of this article. Below, we use the normalization $C_1C_2/c_{\mathrm{SAW}} = 1$; i.e., we consider only the effects of the propagation losses of magnetoelastic waves and the spatial spectra of IDTs, given by F_k.

As was pointed out above, the widths of the magnetoelastic band gaps $\Delta\omega = 2|\kappa_k|$ are several orders of magnitude larger than the SAW linewidth, $\Gamma_{\mathrm{SAW}} \ll \Delta\omega$, and, at the same time, the SW linewidth is typically larger than the width of the magnetoacoustic band gap, $\Gamma_{\mathrm{SW}} > \Delta\omega$. An example of the transmission characteristics calculated for this case is given in Fig. 4. For these calculations, we use the thickness of a polycrystalline Ni layer of $t_{\mathrm{Ni}} = 5$ nm, which is smaller than the optimum thickness, in order to demonstrate that a significant nonreciprocity of the transmission characteristic cannot be achieved only in the unique optimum case. We choose a central frequency of the band gaps of 5 GHz, and the Gilbert damping parameter of the nickel layer is chosen to be $\alpha_G = 0.045$, which is a typical value for polycrystalline Ni films [51]. For these parameters, the spectral widths are $\Gamma_{\mathrm{SAW}}/(2\pi) = 500$ kHz, $\Gamma_{\mathrm{SW}}/(2\pi) = 360$ MHz, and $\Delta\omega = 2|\kappa_k|/(2\pi) = 60$ MHz.

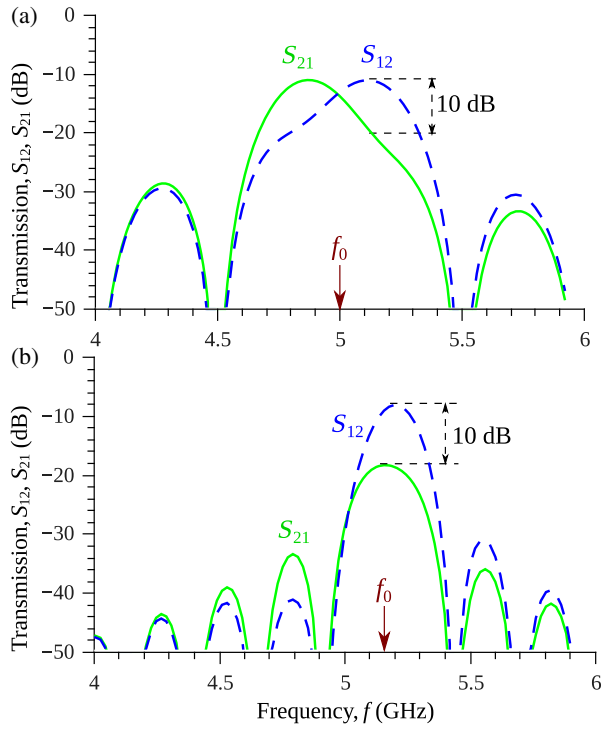

FIG. 4. Transmission characteristics of the SAW lines with a polycrystalline Ni film ($\alpha_G = 0.045$) having different IDTs for the opposite directions of wave propagation [S_{12} (the dashed line) and S_{21} (the solid line)]. (a) IDT1 with central frequency $f_0 = 5$ GHz, number of fingers $N_f = 10$. (b) IDT2 with $f_0 = 5.16$ GHz, $N_f = 20$. The thickness of the Ni layer is $t_{\mathrm{Ni}} = 5$ nm, the SAW line length $L = 250$ μm, and the bias magnetic field $B_e = 82$ mT is applied at the angle $\phi = \pi/4$ to the line axis.

The parameters of the SAW line transmission characteristics can be adjusted by the selection of the IDT central frequency f_0 and the number of IDT fingers. For example, if the IDT central frequency f_0 lies between the magnetoelastic band gaps and the spectrum of the IDT is wide enough to cover both band gaps (a small number of fingers), then the transmission characteristic contains two nonreciprocal bands where the transmission reaches a maximum value at different frequencies for the opposite wave propagation directions [see Fig. 4(a)]. By contrast, if f_0 lies within one of the band gaps and the IDT spectrum is narrow (a large number of fingers), there is one main unidirectional transmission band, as shown in Fig. 4(b). The isolation in both cases is close to 10 dB, while the propagation losses at the transmission maximum do not exceed 10 dB. We note that these values of the isolation are much larger than the ones that were observed for a single Ni film on a $LiNbO_3$ substrate (without Pt) [32], and they can be easily measured and, possibly, used in applications.

The isolation of the SAW line with magnetoelastic coupling can be substantially improved if a high-quality ferromagnetic film is used. As one can show from Eq. (19), the damping of the magnetoelastic waves at the crossing point depends on the relative values of the magnetoelastic coupling coefficient $|\kappa_k|$ and the SW linewidth Γ_{SW}. If $|\kappa_k| > (\Gamma_{\mathrm{SW}} + \Gamma_{\mathrm{SAW}})/2$, the damping rate of the hybridized waves is $\Gamma_{1,2} = (\Gamma_{\mathrm{SW}} - \Gamma_{\mathrm{SAW}})/2$. Otherwise, for $|\kappa_k| < (\Gamma_{\mathrm{SW}} + \Gamma_{\mathrm{SAW}})/2$, the damping rate of the magnetoacoustic waves is equal to $\Gamma_{1,2} = (\Gamma_{\mathrm{SW}} + \Gamma_{\mathrm{SAW}})/2 \pm \sqrt{(\Gamma_{\mathrm{SW}} - \Gamma_{\mathrm{SAW}})^2/4 - |\kappa_k|^2}$, i.e., the damping rate of one of the hybridized magnetoacoustic waves decreases with the increase of Γ_{SW}, and, in the limit $\Gamma_{\mathrm{SW}} \gg |\kappa_k|$, it is reduced to $\Gamma_1 \to \Gamma_{\mathrm{SAW}}$. Naturally, this low-damping hybridized wave makes a dominant contribution to the signal transmission rate, and the isolation in the transmission line decreases in spite of the fact that the signal frequency lies within a magnetoacoustic band gap.

Thus, to maximize the influence of the magnetoelastic coupling on the signal transmission, the SW damping rate should be $\Gamma_{\mathrm{SW}} < 2|\kappa_k|$, while the use of ferromagnetic materials with high magnetic damping leaves SAW transmission almost unaffected.

For the studied heterostructure $LiNbO_3$/Ni/Pt, such an optimum case can be realized if high-quality monocrystalline Ni film is used. In our numerical example illustrated in Fig. 5, we use a high-quality Ni film with a Gilbert damping constant of $\alpha_G = 0.014$ [56]. Here, we choose a Ni layer

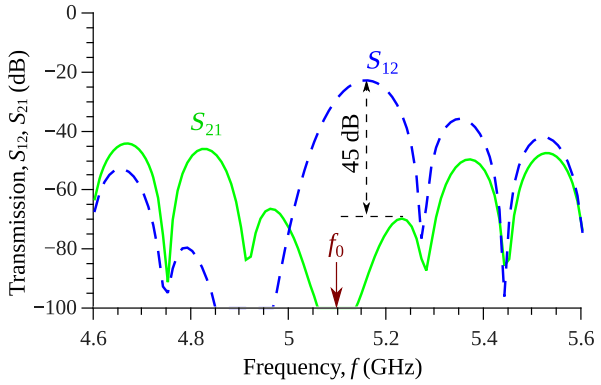

FIG. 5. Transmission characteristics of a SAW line with a monocrystalline Ni film ($\alpha_G = 0.014$) for the opposite directions of wave propagation [S_{12} (the dashed line) and S_{21} (the solid line)]. The thickness of the Ni layer is $t_{\mathrm{Ni}} = 9$ nm, the SAW line length $L = 250$ μm, the IDT central frequency $f_0 = 5.095$ GHz, the number of fingers $N_f = 30$, and the bias magnetic field $B_e = 45$ mT is applied at the angle $\phi = \pi/4$ to the line axis.

thickness of $t_{\mathrm{Ni}} = 9$ nm, for which $2\kappa_k/(2\pi) = 105$ MHz and $\Gamma_{\mathrm{SW}} = 104$ MHz. As is clear from Fig. 5, the isolation in this case is increased remarkably, up to 45 dB, and this isolation also exists in a rather wide frequency band.

It follows from Eq. (20) that the maximum achievable isolation in such a SAW transmission line is on the order of $S_{12} - S_{21} \sim \exp[(\Gamma_{\mathrm{min}} - \Gamma_{\mathrm{SAW}})L/c_{\mathrm{SAW}}]$, where $\Gamma_{\mathrm{min}} = \min \mathrm{Im}[\omega_{1,2}]$ is the smallest damping rate of the hybridized magnetoelastic waves. This maximum isolation is achieved at the frequency in the center of one of the magnetoelastic band gaps, provided that the excitation spectra of the used IDT is sufficiently narrow compared to the band-gap width. The desired IDT bandwidth can be achieved using an IDT with a sufficiently large number of "fingers" N_f.

As was pointed out previously, if the magnetoelastic coupling is relatively weak, $|\kappa_k| < (\Gamma_{\mathrm{SW}} + \Gamma_{\mathrm{SAW}})/2$, we get $\Gamma_{\mathrm{min}} = (\Gamma_{\mathrm{SW}} + \Gamma_{\mathrm{SAW}})/2 - \sqrt{(\Gamma_{\mathrm{SW}} - \Gamma_{\mathrm{SAW}})^2/4 - |\kappa_k|^2}$. In this case, a weak damping of one of the hybridized magnetoelastic waves strongly limits the maximum achievable isolation, and an increase of the number N_f of the IDT fingers does not lead to a significant improvement in the isolation. For example, for the parameters used in Fig. 4(b), the increase of N_f from $N_f = 20$ to $N_f = 100$ gives only 1 dB of the isolation enhancement.

By contrast, in the optimum case of a strong coupling and a high-quality ferromagnetic layer, when $|\kappa_k| > (\Gamma_{\mathrm{SW}} + \Gamma_{\mathrm{SAW}})/2$, the maximum isolation can be very high, so the signal level in one direction can be below the level of a thermal noise. For example, it follows from Fig. 5 that, at the frequency 5.09 GHz, the isolation is 84 dB and can be made even higher for the increased number N_f of IDT fingers. A large number of fingers, however, leads to a severe limitation in the frequency band of the transmitted signal.

Thus, we show here that, by using a well-known acoustic and magnetic material such as $LiNbO_3$ in combination with a Ni film covered by a thin layer of Pt, it is possible to achieve the transmission of hybridized magnetoacoustic waves with quite a large level of nonreciprocal isolation. The characteristics of such a nonreciprocal magnetoacoustic isolator could be further improved by using ferromagnetic materials with lower damping. Promising materials for this purpose could be CoFe alloys, which, at a certain composition, show ultralow magnetic damping of $\alpha_G = 0.0014$ [57]. Unfortunately, the magnetoelastic properties and the DMI of these alloys have not been studied yet.

IV. CONCLUSION

In this work, we present a general theory of linear magnetoelastic coupling between the spin and acoustic waves propagating in an arbitrary magnetic-nonmagnetic layered structure and having arbitrary mode profiles. The developed theory uses the relative weakness of the magnetoelastic interaction and reduces the problem to a standard form of equations for coupled oscillators. The theory provides a simple method for the calculation of the magnetoelastic wave dispersion and the damping parameters of the coupled waves, as well as for the determination of the condition of the nonzero magnetoelastic interaction between the acoustic and spin waves.

Using the developed theory, we demonstrate that the SW nonreciprocity induced by the IDMI can be "transferred" to the "hybridized SAWs" existing in piezoelectric–ferromagnetic–heavy-metal heterostructures. The magnetoelastic interaction results in the appearance of band gaps in the spectra of magnetoelastic surface waves, and, because of the IDMI-induced SW nonreciprocity, these band gaps exist at different frequency and wave-number positions for the opposite wave propagation directions. The widths of these band gaps and the frequency separation between them can be optimized by a proper selection of the in-plane magnetization angle ($\phi \approx \pi/4$ relative to the direction of the SAW propagation) and the thickness of a ferromagnetic layer (about 8 to 9 nm for the studied $LiNbO_3/Ni/Pt$ heterostructure), while the central frequency of the band gaps can be tuned by varying the magnitude of the bias magnetic field.

We demonstrate in this paper that the transmission characteristics of the surface magnetoelastic waves can be substantially nonreciprocal while having relatively low direct insertion losses. Our calculations show that, for $LiNbO_3$ covered by a think Ni/Pt layer, it is possible to achieve an isolation of 10–45 dB while maintaining the SAW propagation losses below 10–20 dB. The isolation could be further improved by a selection of a proper ferromagnetic material having large values for the magnetostriction and the IDMI, but low magnetic losses.

ACKNOWLEDGMENTS

This work was supported in part by a grant from the Center for NanoFerroic Devices (CNFD) and the Nanoelectronics Research Initiative (NRI), by Grants No. EFMA-1641989 and No. ECCS-1708982 from the U.S. NSF, and by the DARPA M3IC grant under Contract No. W911-17-C-0031. R. V. acknowledges support from the Ministry of Education and Science of Ukraine (Project No. 0118U004007). I. L. acknowledges support from DARPA SPAR (Grant No. HR0011-17-2-2005) and the Russian Science Foundation (Project No. 14-19-00760).

[1] C. Campbell, *Surface Acoustic Wave Devices and Their Signal Processing Applications* (Academic Press, New York, 1989).

[2] B. A. Auld, *Acoustic Fields and Waves in Solids* (Krieger Publishing, Malabar, FL, 1990).

[3] D. Morgan, *Surface Acoustic Wave Filters: With Applications to Electronic Communications and Signal Processing*, 2nd ed., Studies in Electrical and Electronic Engineering (Academic Press, London, 2010).

[4] E. A. Ash, A. A. Oliner, G. W. Farnell, H. M. Gerard, A. A. Oliner, A. J. Slobodnik, and H. I. Smith, in *Acoustic Surface Waves*, edited by A. A. Oliner, Topics in Applied Physics Vol. 24 (Springer, Berlin, 2014).

[5] A. G. Gurevich and G. A. Melkov, *Magnetization Oscillations and Waves* (CRC Press, New York, 1996).

[6] B. K. Kuanr, V. Veerakumar, R. Marson, S. R. Mishra, R. E. Camley, and Z. Celinski, Nonreciprocal microwave devices based on magnetic nanowires, Appl. Phys. Lett. **94**, 202505 (2009).

[7] J. Heil, B. Lüthi, and P. Thalmeier, Nonreciprocal surface-acoustic-wave propagation in aluminum, Phys. Rev. B **25**, 6515 (1982).

[8] R. Fleury, D. L. Sounas, C. F. Sieck, M. R. Haberman, and A. Alù, Sound isolation and giant linear nonreciprocity in a compact acoustic circulator, Science **343**, 516 (2014).

[9] B. Liang, B. Yuan, and J.-C. Cheng, Acoustic Diode: Rectification of Acoustic Energy Flux in One-Dimensional Systems, Phys. Rev. Lett. **103**, 104301 (2009).

[10] B. Liang, X. S. Guo, J. Tu, D. Zhang, and J. C. Cheng, An acoustic rectifier, Nat. Mater. **9**, 989 (2010).

[11] N. Boechler, G. Theocharis, and C. Daraio, Bifurcation-based acoustic switching and rectification, Nat. Mater. **10**, 665 (2011).

[12] Z.-M. Gu, J. Hu, B. Liang, X.-Y. Zou, and J.-C. Cheng, Broadband non-reciprocal transmission of sound with invariant frequency, Sci. Rep. **6**, 19824 (2016).

[13] J. R. Eshbach and R. W. Damon, Surface magnetostatic modes and surface spin waves, Phys. Rev. **118**, 1208 (1960).

[14] G. A. Melkov, V. I. Vasyuchka, V. V. Lazovskiy, V. S. Tiberkevich, and A. N. Slavin, Wave front reversal with frequency conversion in a nonreciprocal medium, Appl. Phys. Lett. **89**, 252510 (2006).

[15] M. Mruczkiewicz, M. Krawczyk, G. Gubbiotti, S. Tacchi, Yu. A. Filimonov, D. V. Kalyabin, I. V. Lisenkov, and S. A. Nikitov, Nonreciprocity of spin waves in metallized magnonic crystal, New J. Phys. **15**, 113023 (2013).

[16] R. Verba, V. Tiberkevich, E. Bankowski, T. Meitzler, G. Melkov, and A. Slavin, Conditions for the spin wave nonreciprocity in an array of dipolarly coupled magnetic nanopillars, Appl. Phys. Lett. **103**, 082407 (2013).

[17] I. Lisenkov, V. Tyberkevych, A. Slavin, P. Bondarenko, B. A. Ivanov, E. Bankowski, T. Meitzler, and S. Nikitov, Spin-wave edge modes in finite arrays of dipolarly coupled magnetic nanopillars, Phys. Rev. B **90**, 104417 (2014).

[18] R. Verba, E. Bankowski, T. Meitzler, V. Tiberkevich, and A. Slavin, Nonreciprocal spin waves in a magnonic crystal with in-plane static magnetization, SPIN **06**, 1640013 (2016).

[19] R. L. Melcher, Linear Contribution to Spatial Dispersion in the Spin-Wave Spectrum of Ferromagnets, Phys. Rev. Lett. **30**, 125 (1973).

[20] D. Cortés-Ortuño and P. Landeros, Influence of the Dzyaloshinskii-Moriya interaction on the spin-wave spectra of thin films, J. Phys. Condens. Matter **25**, 156001 (2013).

[21] J.-H. Moon, S.-M. Seo, K.-J. Lee, K.-W. Kim, J. Ryu, H.-W. Lee, R. D. McMichael, and M. D. Stiles, Spin-wave propagation in the presence of interfacial Dzyaloshinskii-Moriya interaction, Phys. Rev. B **88**, 184404 (2013).

[22] V. L. Zhang, K. Di, H. S. Lim, S. C. Ng, M. H. Kuok, J. Yu, J. Yoon, X. Qiu, and H. Yang, In-plane angular dependence of the spin-wave nonreciprocity of an ultrathin film with Dzyaloshinskii-Moriya interaction, Appl. Phys. Lett. **107**, 022402 (2015).

[23] M. Tsutsumi, T. Bhattacharyya, and N. Kumagai, Piezoelectricmagnetoelastic surface wave guided by interface between semiinfinite piezoelectric and magnetoelastic media, J. Appl. Phys. **46**, 5072 (1975).

[24] G. Komoriya and G. Thomas, Magnetoelasticsurface waves on YIG substrate, J. Appl. Phys. **50**, 6459 (1979).

[25] Y. Shimizu, K. Hasegawas, and T. Yamada, Nonreciprocity of SAW velocity on a magnetized ferrite substrate, Electron. Commun. Jpn., Part I **63**, 1 (1980).

[26] C. Kittel, Interaction of spin waves and ultrasonic waves in ferromagnetic crystals, Phys. Rev. **110**, 836 (1958).

[27] K. B. Vlasov, Equations of motion for magnetization in deformed anisotropic media, Sov. Phys. JETP **16**, 1505 (1963).

[28] R. L. Comstock, Parallel pumping of magnetoelastic waves in ferromagnets, J. Appl. Phys. **35**, 2427 (1964).

[29] M. Weiler, L. Dreher, C. Heeg, H. Huebl, R. Gross, M. S. Brandt, and S. T. B. Goennenwein, Elastically Driven Ferromagnetic Resonance in Nickel Thin Films, Phys. Rev. Lett. **106**, 117601 (2011).

[30] P. G. Gowtham, T. Moriyama, D. C. Ralph, and R. A. Buhrman, Traveling surface spin-wave resonance spectroscopy using surface acoustic waves, J. Appl. Phys. **118**, 233910 (2015).

[31] V. Polewczyk, K. Dumesnil, D. Lacour, M. Moutaouekkil, H. Mjahed, N. Tiercelin, S. Petit Watelot, H. Mishra, Y. Dusch, S. Hage-Ali, O. Elmazria, F. Montaigne, A. Talbi, O. Bou Matar, and M. Hehn, Unipolar and Bipolar High-Magnetic-Field Sensors Based on Surface Acoustic Wave Resonators, Phys. Rev. Applied **8**, 024001 (2017).

[32] R. Sasaki, Y. Nii, Y. Iguchi, and Y. Onose, Nonreciprocal propagation of surface acoustic wave in Ni/$LiNbO_3$, Phys. Rev. B **95**, 020407 (2017).
[33] P. G. Gowtham, T. Moriyama, D. C. Ralph, and R. A. Buhrman, Traveling surface spin-wave resonance spectroscopy using surface acoustic waves, J. Appl. Phys. **118**, 233910 (2015).
[34] X. Li, D. Labanowski, S. Salahuddin, and C. S. Lynch, Spin wave generation by surface acoustic waves, J. Appl. Phys. **122**, 043904 (2017).
[35] R. Duflou, F. Ciubotaru, A. Vaysset, M. Heyns, B. Sorée, I. P. Radu, and C. Adelmann, Micromagnetic simulations of magnetoelastic spin wave excitation in scaled magnetic waveguides, Appl. Phys. Lett. **111**, 192411 (2017).
[36] A. Barra, A. Mal, G. Carman, and A. Sepulveda, Voltage induced mechanical/spin wave propagation over long distances, Appl. Phys. Lett. **110**, 072401 (2017).
[37] V. V. Naletov, G. de Loubens, G. Albuquerque, S. Borlenghi, V. Cros, G. Faini, J. Grollier, H. Hurdequint, N. Locatelli, B. Pigeau, A. N. Slavin, V. S. Tiberkevich, C. Ulysse, T. Valet, and O. Klein, Identification and selection rules of the spin-wave eigenmodes in a normally magnetized nanopillar, Phys. Rev. B **84**, 224423 (2011).
[38] R. Verba, G. Melkov, V. Tiberkevich, and A. Slavin, Collective spin-wave excitations in a two-dimensional array of coupled magnetic nanodots, Phys. Rev. B **85**, 014427 (2012).
[39] O. Dzyapko, I. Lisenkov, P. Nowik-Boltyk, V. E. Demidov, S. O. Demokritov, B. Koene, A. Kirilyuk, T. Rasing, V. Tiberkevich, and A. Slavin, Magnon-magnon interactions in a room-temperature magnonic Bose-Einstein condensate, Phys. Rev. B **96**, 064438 (2017).
[40] S. Chikazumi, *Physics of Ferromagnetism*, International Series of Monographs on Physics Vol. 94 (Oxford University Press, New York, 2009).
[41] Making a comparison to Refs. [37–39], here we add the dimensional multiplier M_s/γ, which aligns the units of the spin-wave norm with the same units as the acoustic normalization constant.
[42] D. Kalyabin, I. Lisenkov, Y. P. Lee, and S. Nikitov, Frequency separation of surface acoustic waves in layered structures with acoustic metamaterials, Photonics Nanostruct. Fundam. Appl. **12**, 239 (2014).
[43] T. Brächer, O. Boulle, G. Gaudin, and P. Pirro, Creation of unidirectional spin-wave emitters by utilizing interfacial Dzyaloshinskii-Moriya interaction, Phys. Rev. B **95**, 064429 (2017).
[44] M. Kostylev, Interface boundary conditions for dynamic magnetization and spin wave dynamics in a ferromagnetic layer with the interface Dzyaloshinskii-Moriya interaction, J. Appl. Phys. **115**, 233902 (2014).
[45] *Acoustic Surface Waves*, edited by A. A. Oliner (Springer, New York, 1978).
[46] Pawe Sobieszczyk, Mirosaw Gazka, Dominik Trzupek, and Piotr Zieliski, Propagation of surface waves and surface resonances along cylindrical cavities in materials with any allowed Poisson's ratio—Part I: Clean inner surface, Phys. Status Solidi (b) **252**, 1595 (2015).
[47] S. Tacchi, R. E. Troncoso, M. Ahlberg, G. Gubbiotti, M. Madami, J. Åkerman, and P. Landeros, Interfacial Dzyaloshinskii-Moriya Interaction in Pt/CoFeB Films: Effect of the Heavy-Metal Thickness, Phys. Rev. Lett. **118**, 147201 (2017).
[48] L. D. Landau, L. P. Pitaevskii, A. M. Kosevich, and E. M. Lifshitz, *Theory of Elasticity*, Course of Theoretical Physics Vol. 7 (Butterworth-Heinemann, Oxford, 2012).
[49] X. Chen, M. Mohammad, J. Conway, B. Liu, Y. Yang, and T.-L. Ren, High performance lithium niobate surface acoustic wave transducers in the 4–12 GHz super high frequency range, J. Vac. Sci. Technol. B **33**, 06F401 (2015).
[50] A. S. Andrushchak, B. G. Mytsyk, H. P. Laba, O. V. Yurkevych, I. M. Solskii, A. V. Kityk, and B. Sahraoui, Complete sets of elastic constants and photoelastic coefficients of pure and MgO-doped lithium niobate crystals at room temperature, J. Appl. Phys. **106**, 073510 (2009).
[51] J. Walowski, M. Djordjevic Kaufmann, B. Lenk, C. Hamann, J. McCord, and M. Münzenberg, Intrinsic and non-local Gilbert damping in polycrystalline nickel studied by Ti:sapphire laser fs spectroscopy, J. Phys. D **41**, 164016 (2008).
[52] D. Sander, The correlation between mechanical stress and magnetic anisotropy in ultrathin films, Rep. Prog. Phys. **62**, 809 (1999).
[53] G. Chen, T. Ma, A. T. N'Diaye, H. Kwon, C. Won, Y. Wu, and A. Schmid, Tailoring the chirality of magnetic domain walls by interface engineering, Nat. Commun. **4**, 2671 (2013).
[54] W. S. Wilson and G. M. Atkinson, A comparison of surface acoustic wave modeling methods, in *Nanotechnology 2009: Biofuels, Renewable Energy, Coatings, Fluidics and Compact Modeling*, Vol. 3 (Nano Science and Technology Institute, Danville, CA, 2009), p. 347.
[55] K. Yamanouchi, Generation, propagation, and attenuation of 10 GHz-range SAW in $LiNbO_3$, in *Proceedings of the 1998 IEEE Ultrasonics Symposium (Cat. No. 98CH36102), Sendai, Japan, 1998*, edited by S. C. Schneider, M. Levy, and B. R. McAvoy (IEEE, New York, 1998), Vol. 1, p. 57, DOI: 10.1109/ULTSYM.1998.762099.
[56] N. Inaba, H. Asanuma, S. Igarashi, S. Mori, F. Kirino, K. Koike, and H. Morita, Damping Constants of Ni-Fe and Ni-Co Alloy Thin Films, IEEE Trans. Magn. **42**, 2372 (2006).
[57] A. J. Lee, J. T. Brangham, Y. Cheng, S. P. White, W. T. Ruane, B. D. Esser, D. W. McComb, P. C. Hammel, and F. Yang, Metallic ferromagnetic films with magnetic damping under 1.4×10^{-3}, Nat. Commun. **8**, 234 (2017).